2011-12-13

Mechanics of Expanding Grout Based Grips for Large Scale Composites Testing

Derek G. Schesser
University of Miami, d.schesser@umiami.edu

UNIVERSITY OF MIAMI

MECHANICS OF EXPANDING GROUT BASED GRIPS FOR LARGE SCALE COMPOSITES TESTING

By

Derek G. Schesser

A THESIS

Submitted to the Faculty
of the University of Miami
in partial fulfillment of the requirements for
the degree of Master of Science

Coral Gables, Florida

December 2011

UNIVERSITY OF MIAMI

A thesis submitted in partial fulfillment of
the requirements for the degree of
Master of Science

MECHANICS OF EXPANDING GROUT BASED GRIPS FOR LARGE SCALE COMPOSITES TESTING

Derek G. Schesser

Approved:

____
Qingda Yang, Ph.D.
Asst. Professor of
Mechanical and Aerospace Engineering

____
Terri A. Scandura, Ph.D.
Dean of the Graduate School

____
Jizhou Song, Ph.D.
Asst. Professor of
Mechanical and Aerospace Engineering

____
Antonio Nanni, Ph.D.
Professor and Chair of
Civil, Architectural, and Environmental Engineering

SCHESSER, DEREK (M.S., Mechanical Engineering)
Mechanics of Expanding Grout Based Grips for Large Scale Composites Testing (December 2011)

Abstract of a thesis at the University of Miami.

Thesis supervised by Professor Qingda Yang.
No. of pages in text. (44)

Experimental testing of large composite specimens under tension or shear is inherently challenging because the large required gripping force and resulting local stress concentration tend to break specimens near gripping sites, rather than desired gage sections. A method using expansive grout materials has been proposed since the mid 1990's. However, there has been no well-established design guideline due to lack of understanding of the gripping pressure developed by the expansive grout material. Key properties including the elastic modulus and linear expansion coefficient are difficult to measure because typical grout materials do not consolidate into coherent solid blocks for traditional property measurement.

In this study, the elastic modulus and linear expansion coefficient of an expansive grout material have been indirectly measured through a carefully designed cylindrical system. The expansive grout material is let to expand within thick-walled steel pipes with one end capped and the other end free to the atmosphere. An analytical solution has been derived to correlate the hoop strain on the outer surface of the steel pipe (caused by grout expansion in the pipe) to the grout elastic modulus and linear expansion coefficient. By measuring the exterior surface hoop strains of two different steel pipes, the elastic modulus and linear expansion coefficient have been determined using the analytical solution of thick walled cylinders. With these parameters accurately determined, the

interface friction coefficient has been estimated through analyzing actual composite specimen tests. Finally, based on the determined parameters and the analytical solution, an improved design procedure has been proposed.

ACKNOWLEDGMENTS

I wish to express sincere appreciation to Professors Q. D. Yang and A. Nanni for their assistance in the preparation of this manuscript. In addition, thanks to Composites Research Technologies Inc. for its support and initial motivation for understanding this gripping technique in detail.

TABLE OF CONTENTS

LIST OF FIGURES v
LIST OF TABLES vi

CHAPTER 1: INTRODUCTION 1

1.1 GENERAL ASPECTS OF COMPOSITE MATERIALS 1
1.2 MECHANICAL BEHAVIOR OF COMPOSITE MATERIALS 3
1.3 COMPOSITE TESTING 4
1.4 STATEMENT OF PROBLEM 7
1.5 RESEARCH OBJECTIVES 8

CHAPTER 2: BACKGROUND AND PROPOSED RESEARCH 9

2.1 GRIPPING MECHANICS 9
2.2 DESIGN CONSIDERATION OF GRIPS FOR COMPOSITES TESTING 11
2.3 PROPOSED METHOD FOR DETERMINING GROUT MODULUS AND LINEAR EXPANSION COEFFICIENT 14

CHAPTER 3: EXPERIMENTAL RESULTS 21

3.1 TEST SETUP 21
3.2 EXPERIMENTAL RESULTS 24

CHAPTER 4: APPLICATION TO SPECIMEN DESIGN 29

4.1 ANALYTICAL GROUNDWORK 29
4.2 REAL APPLICATIONS 34

CHAPTER 5: CONCLUSIONS AND RECOMMENDATIONS 38

5.1 DESIGN GUIDELINES 38
6.2 DESIGN GUIDELINE EXAMPLE 42
6.3 DESIGN CONCLUSIONS 43

BIBLIOGRAPHY 44

LIST OF FIGURES

Figure 1 Traditional tensile test wedge grip 10

Figure 2 Grout filled grip 11

Figure 3. Recommended anchor system ASTM D 7205 Annex A1................................13

Figure 4 Cylindrical setup...15

Figure 5 Deformations due to pressure 17

Figure 6 Radii definitions $r_i = b$ and $r_o = c$ 17

Figure 7 Strain gauge layout 22

Figure 8 Pipe filled with grout 23

Figure 9 NI cDAQ-9174 24

Figure 10 Data strain versus time 25

Figure 11 Cross Section with composite specimen 29

Figure 12 New radii definitions 30

Figure 13 Test setup...35

Figure 14 Anchorage to test machine 36

Figure 15 Optimal grout shell thickness 36

Figure 16 Grout-Composite Pressure vs. Composite Radii 39

Figure 17 Pipe length chart 40

Figure 18 Example pipe design...42

LIST OF TABLES

Table 1 Pipe sizes....23

Table 2 Strain for the Large-Medium system....26

Table 3 Strain for Medium-Small system....27

Table 4 Effective friction coefficients....35

CHAPTER 1: INTRODUCTION

1.1 General Aspects of Composite Materials

Composites as the name suggests consists of two or more materials combined into one. The resulting material has properties that are a combination of the properties of the constituent materials. There are four common accepted types of composite materials (Jones, 1999):

1. *Fibrous* composites where fibers are embedded in a matrix
2. *Laminated* composites where layers of different materials are stacked
3. *Particulate* composite where particles are incased in matrix
4. Combinations of all or some of the above

Fibrous composites are the focus of the work presented here. Long fibers can have properties much different than the same material in bulk form. This is the case with glass, where the strength of bulk glass is on the order of 20 MPa while glass fiber's strength can reach 4800 MPa (Jones, 1999). This is due to the fact that in the fiber form the material on the atomic scale is arranged in a more perfect structure; crystals are in alignment with the fiber axis. This results in fewer defects or dislocations than is normally present in bulk form. However, from a structural perspective, in fibrous form with fiber diameters between five and ten micrometers the material is very flexible. To use these fibers as a structural element they must be embedded in a matrix material that provides stress transfer between fibers.

Most commercial applications use a polymer based resin as a matrix. The make-ups of these resins vary considerably and are carefully selected based upon the application. Common resins include Polyester, Vinyl ester, and Epoxy. Polyester resin tends to be yellowish, its main disadvantage is its sensitivity to ultraviolet radiation which causes it to degrade over time. But it is very easy to use and usually the constituents of the resin provide the necessary heat to perform the crosslinking process required for curing. Vinyl ester is usually purple or bluish and has a lower viscosity which helps with fiber impregnation and is slightly more durable than polyester resin. Epoxy is another resin that is widely used and is completely transparent when cured. There are countless combinations and variations of composition in the modern composites industry. Composites can be tailored to very specific applications, to a higher degree than metals. The work presented here involves glass fiber reinforced with a vinyl ester matrix.

Fibrous composites offer many advantages over traditional materials, in recent years composites have seen new and ever growing applications in all areas of engineering. A widespread application of composite rods is in civil engineering, for the pre or post tensioning of concrete. This is critical in advanced concrete structures as it utilizes concrete's high compressive strength by applying a compressive force, thereby avoiding or reducing any tensile stresses in the concrete. Composite rods offer an excellent solution over steel due to their non-corrosive properties, excellent fatigue performance, lightweight, and high strengths (A. Al-Mayah, 2007). In the aerospace industry composites offer significant advantages due to their high strength to weight ratios (Daniel, 2006). New more efficient airplanes are becoming more and more composed of composites. Currently the commercial passenger airplane that has the highest percentage of composites is the Boeing 787 "Dreamliner". In the biomedical field composites are used almost exclusively for prosthesis.

1.2 Mechanical Behavior of Composite Materials

Composite materials differ greatly in mechanical behavior when compared to conventional engineering materials. Due to these differences the problem of their mechanics must be approached from the lowest level and built up. Most engineering materials are isotropic; this means they exhibit the same properties regardless of direction. In contrast, composite materials are both anisotropic and nonhomogeneous, more commonly referred to as orthotropic and heterogeneous. This means in general composite material properties depend both on direction and location. Because of this heterogeneity, composites are studied at two levels:

1. The micromechanics level where the interactions between constituent materials are examined
2. The macromechanics level where the properties of the composite are treated as a whole

From a design perspective it is the macromechanics that are of most importance. Macromechanical or structural properties of a composite require at most twenty-one independent constants to be fully characterized in the case of a fully anisotropic composite. More common however are orthotropic (9 independent constants) and transversely isotropic (5 independent constants) composite materials.

The stress-strain matrix representation of a composite in its most general form is presented below:

$$\begin{bmatrix} \varepsilon_1 \\ \varepsilon_2 \\ \varepsilon_3 \\ \gamma_{23} \\ \gamma_{31} \\ \gamma_{12} \end{bmatrix} = \begin{bmatrix} S_{11} & S_{12} & S_{13} & S_{14} & S_{15} & S_{16} \\ S_{11} & S_{22} & S_{23} & S_{24} & S_{25} & S_{26} \\ S_{13} & S_{23} & S_{33} & S_{34} & S_{35} & S_{36} \\ S_{14} & S_{24} & S_{34} & S_{44} & S_{45} & S_{46} \\ S_{15} & S_{25} & S_{35} & S_{45} & S_{55} & S_{56} \\ S_{16} & S_{26} & S_{36} & S_{46} & S_{56} & S_{66} \end{bmatrix} \begin{bmatrix} \sigma_1 \\ \sigma_2 \\ \sigma_3 \\ \tau_{23} \\ \tau_{31} \\ \tau_{12} \end{bmatrix} \tag{1}$$

As can be seen from this relation multiple coupling mechanisms can exist. This becomes problematic if a traditional approach is taken for design and testing.

1.3 Composite Testing

Knowing how a material behaves when stressed to its breaking point is very important in engineering design. In the case of isotropic materials such as structural metals it is relatively straightforward as the material properties are identical for all loading directions. It becomes more complicated with anisotropic or orthotropic composites because their material properties are directional. For such materials, tests must be performed along multiple loading directions to determine the property dependence on orientation. For example, for a simple unidirectional fiber specimen, tension and compression tests along the fiber direction as well as transverse to the fiber direction are needed. Shear modulus and shear strength tests are less straight forward as it is difficult to produce a pure shear condition in the specimen.

For a good test the following criteria must be considered (Jones, 1999):

1. The highest stress must occur in the gage section to insure failure in this region

2. A uniform stress field must exist over the entire gage section volume to eliminate volume based statistical failures

3. Unwanted stresses must be eliminated as much as possible from the gage section

These criteria are a bare minimum to be considered when designing a test. For the type of testing done in the research presented here ASTM D 7205 provides a guideline for parameters such as sampling rate, loading rate, environmental factors, and reporting procedures. It also contains in its annex the recommended anchor system that was implemented in the testing presented later as part of the application of this work. For the successful use of composites the primary fiber direction strength as stated before is a fundamental characterization that must be performed.

Much of the research and development therefore consist of developing new gripping methods, with no single method prevailing (Gilstrap, 2001). The mechanisms of load transfer vary between different designs but they can be categorized in two distinct groups. The first group transfers load by applying a clamping force and relies on the interface interaction. If this clamping force is applied uniformly then a high shear stress will develop at the loaded end. This led to work which sought to introduce a stiffness gradient in the grip itself where the loaded end of the grip had a softer material to reduce the stress concentrations (Meier, 1995). The second group relies on the underlying principle of the traditional wedge grip with various augmentations to mitigate the loaded end shear stress concentrations (Carvelli, 2009). The commonality between the research done for both groups of gripping methods has been that the experimental work far outweighs the analytical analysis. The synergy between experimental tests and mechanical modeling is well established in other fields and was recommended for the development of composite anchors (Rostàsy, 1993). These designs are many, and varied in approach but all seek the same goal.

However, for composite materials, due to the fact that their strength in the primary fiber direction is usually much larger than the transverse direction, traditional wedge type gripping methods, even with load-end stress mitigation treatments, are not well suited for large composite specimen testing. The large gripping force needed to fail a specimen in the primary fiber direction is applied in the transverse direction of a specimen (typically weaker direction). Most of the time this causes local failure near the gripping site rather than the desired gage section. The situation is exacerbated by the local stress concentration at the gripping site if traditional wedge type grips are used (G. Portnov, 2008).

Presently alternative techniques for gripping have been largely individualized sub-projects that many times prove time consuming and result in varying degrees of success. As a result a large number of specialized gripping systems have been developed. For example, an ASTM recommended system involves the use of steel tubes filled with expansive grout. The configuration of the anchor is such that the grout forms a cylindrical shell around the specimen. After curing the expansive grout exerts a pressure on the specimen and facilitates testing, leading to failure in the gage section. The clamping pressure exerted on the specimen is dependent on the confinement provided by the steel pipe, the thickness of the grout layer, modulus, and expansion coefficient of the expansive grout material.

The mechanics of these anchors are not well understood. Due to the expansive nature of the grout it is impossible to create specimens that are homogeneous to directly measure the modulus. Traditionally, cubes would be made to test the expansive grout properties as per ASTM C109. It has been shown that expansive grout when placed in two inch metal molds will destroy the molds as well as spread a very fine powder over the surrounding area (Tibbets, 2008).

Without knowing the grout modulus and linear expansion coefficient, it is impossible to calculate the clamping pressure that will develop in such an anchoring system. Currently a trial and error design methodology has to be applied, which is very inefficient.

1.4 Statement of Problem

As discussed above, to successfully reach the ultimate strength of large scale composite specimens requires anchor (gripping) systems that are able to grip the tendon without causing failure in the tendon near the grip. Traditional wedge type gripping systems have proven to be insufficient in large composite specimen testing because the large gripping force required and resulting local stress concentration tend to initiate failure in the specimen near the gripping sites, rather than the desired gage sections.

This study aims to develop a method that can determine the grout material properties including Young's modulus and linear expansion coefficient using a cylindrical system that is similar to the ASTM recommended configuration for actual composite testing. The basic idea is to let the grout material expand within thick-walled steel pipes with one end capped and the other end free to expand. Measurement of the hoop strain at the outer surface of the steel pipes, which is caused by the grout material expansion, should provide useful information for calculation of the grout material properties. It is anticipated that based on the determined parameters and the analytical solution, an improved design procedure can be derived.

1.5 Research Objectives

The objectives of this study are to provide an improved understanding of the complex mechanics problem associated with gripping composites with expanding grout based grips. Knowing how the system dimensions affect the stresses developed within the grip will enable future grips to be designed more quickly and more material efficiently. This will lead to significant monetary savings for future material characterizations studies and quality control protocols.

CHAPTER 2: BACKGROUND AND PROPOSED RESEARCH

2.1 Gripping Mechanics

A successful grip is one that can transfer sufficient load to facilitate failure in the gage section. This is typically done by enlarging the grip regions known as the tab regions, which lowers the stresses in these regions and prevents failure at or near the grip. The specimen must then transition from the tab dimension to the smaller gage section dimension, this must be done gradually to reduce any stress concentrations that occur at sudden changes of cross sectional area. When working with epoxy-glass composites the transverse strength is significantly lower than the strength in the primary fiber direction. As a result gripping pressure can crush the specimen in the transverse direction if it is applied indiscriminately. Traditional grips use a component of the tensile force to help grip the specimen, these are called wedge grips. The more tension that is applied, the more the wedge grip squeezes the specimen. With composites this can be problematic due to the large tensile forces needed to reach ultimate stress levels in the fiber direction combined with the weaker transverse strength.

Once it is established that enough gripping pressure can be applied to fail the specimen, consideration must be made for the stress concentrations that develop at the loaded end.

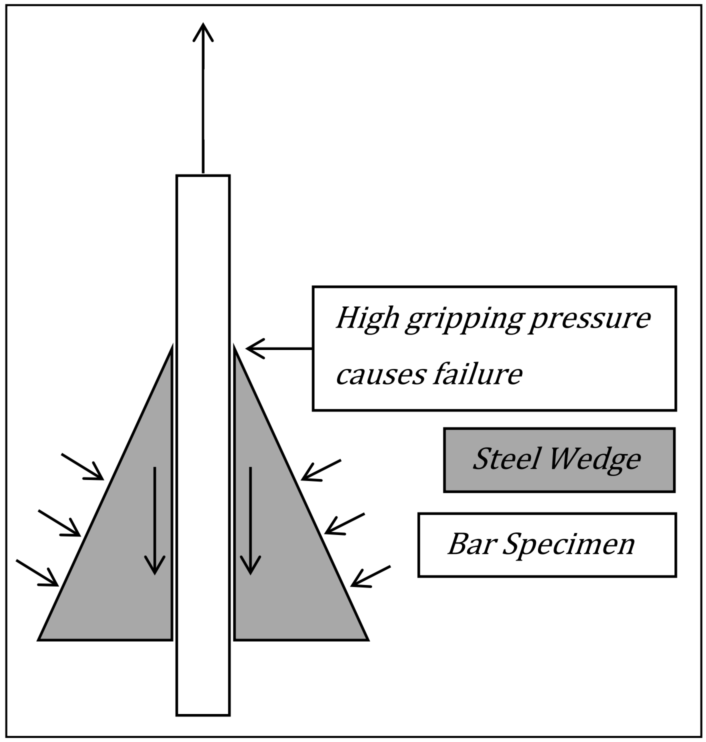

Figure 1 Traditional tensile test wedge grip

The gripping force is applied through friction on the surface of the specimen. It becomes a delicate balance to apply enough gripping pressure to facilitate the friction needed for testing while not crushing the specimen in the grip. In the case of wedge grips this can be achieved by changing the wedge shape and/or introducing a secondary material between the specimen and wedge, as shown in Figure 1.

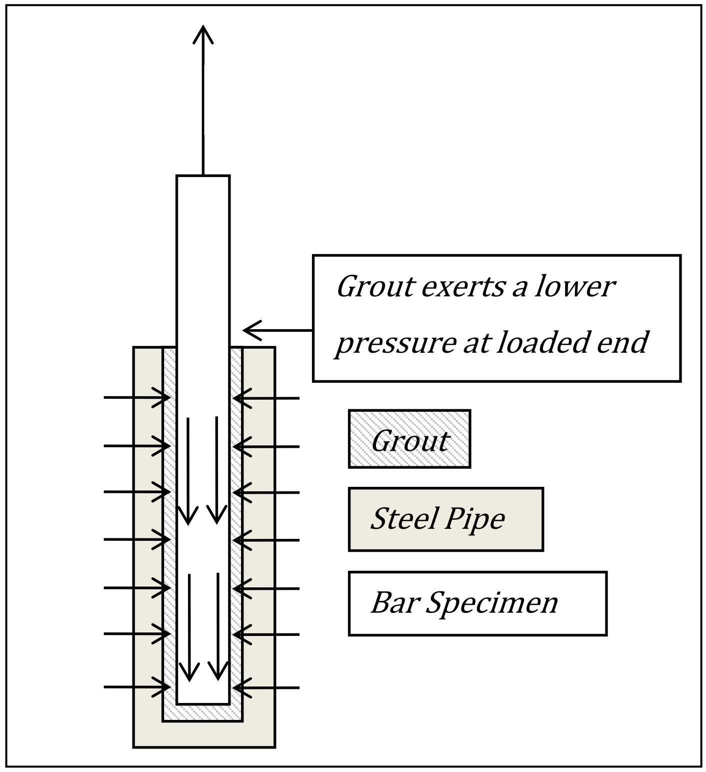

Figure 2 Grout filled grip

In the case of the expansive grout based grip, shown in Figure 2 a steel pipe is filled with expanding grout and a composite specimen placed in its center. The grout is allowed to cure, exerting a pressure force on the inside surface of the pipe and the outside surface of the specimen. When the test is performed the gripping pressure is independent of the tension applied.

2.2 Design Consideration of Grips for Composites Testing

The most important aspect of a grip is to allow sufficient load to be transferred to the gage section so that failure occurs within the gage section. As stated earlier with composites this represents a great challenge due to the large disparity in properties depending on the orientation of applied load. For tensile tests that were performed later in this work, the force is transferred though a shear force f, also called unit area friction force, that is developed on the surface of the specimen. This friction force is proportional to the gripping pressure applied to the specimen by a material specific friction coefficient, μ.

$$f = \mu P \tag{2}$$

$$F = fA = \mu PA \tag{3}$$

where A is the total area that is active in providing the unit area friction force. Note that here it is implicitly assumed that the unit area friction force is uniform throughout the active zone.

From this it is clear that we need simply to hold the specimen as tight as possible and we will have a friction force high enough to reach the failure stress levels in the specimen. Although that is not the only consideration because going forward in this manner will very likely result in the failure stress occurring first in or near the grip before the ultimate stress level is reached in the gage section. This gripping or normal pressure must be applied over a sufficiently large area to reduce the stress levels while providing adequate friction. One advantage of the expansive grout based grip is that one can adjust the grout material layer thickness and specimen embedment length to accommodate the needed clamping pressure. However, to achieve such a design, accurate assessment of the gripping pressure as functions of steel pipe dimensions and grout material thickness (volume) is needed. This is the primary focus of this study.

Another critical criterion is then to have a grip configuration that can be held in the testing frame to be used. The methods for securing the grip to the testing machine are varied but as a general outline the grips must be mounted or gripped in such a way that the specimen grips are not damaged or introduce any pressures that are detrimental to the grip performance. With this view the grips for composites are in fact two grip systems that are coupled in such a way to facilitate testing. ASTM D 7205 provides in its Annex A1 a recommended anchor system as shown in Figure 3. It is noted that other methods can be used if it can be demonstrated to facilitate failure away from the grip as well as limiting excessive slip before failure.

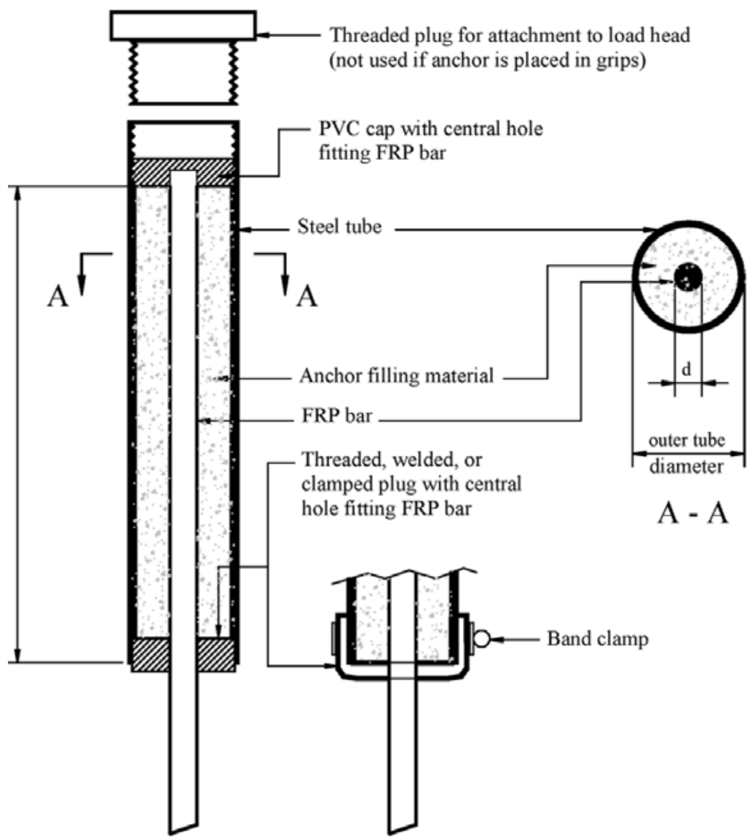

Figure 3. Recommended anchor system ASTM D 7205 Annex A1

2.3 Proposed Method for Determining Grout Modulus and Linear Expansion Coefficient

Due to the expansive nature of the expansive grout material, it is impossible to determine its properties by consolidating the grout material into well-shaped material blocks for standard testing such as ASTM C109. In this study, a combined analytical and experimental approach will be explored to deduce material properties. The problem focused on here is a thick walled cylinder under internal and external pressure as shown in Figure 4. The internal pressure p_i is directly due to the confined expansion of the grout material, which fills in the entire interior space of the steel pipe. The problem is an axial symmetric one and assuming plane strain condition the governing differential equation is given by (Budyas 1999):

$$r\left(\frac{d^2\sigma_r}{dr^2}\right)+3\left(\frac{d\sigma_r}{dr}\right)=0 \tag{4}$$

The general solution for the stress components in the steel pipe are:

$$\sigma_r\left(r\right)=\frac{P_ir_i^2-P_or_o^2+\left(\frac{r_ir_o}{r}\right)^2(P_o-P_i)}{r_o^2-r_i^2} \tag{5}$$

$$\sigma_\theta\left(r\right)=\frac{P_ir_i^2-P_or_o^2-\left(\frac{r_ir_o}{r}\right)^2\left(P_o-P_i\right)}{r_o^2-r_i^2} \tag{6}$$

where Eq. (5) and Eq. (6) are the radial and hoop stress, respectively. For a plane strain condition, a uniform axial stress σ_z also exists.

$$\sigma_z=-2\nu\frac{P_ir_i^2-P_or_o^2}{r_i^2-r_o^2} \tag{7}$$

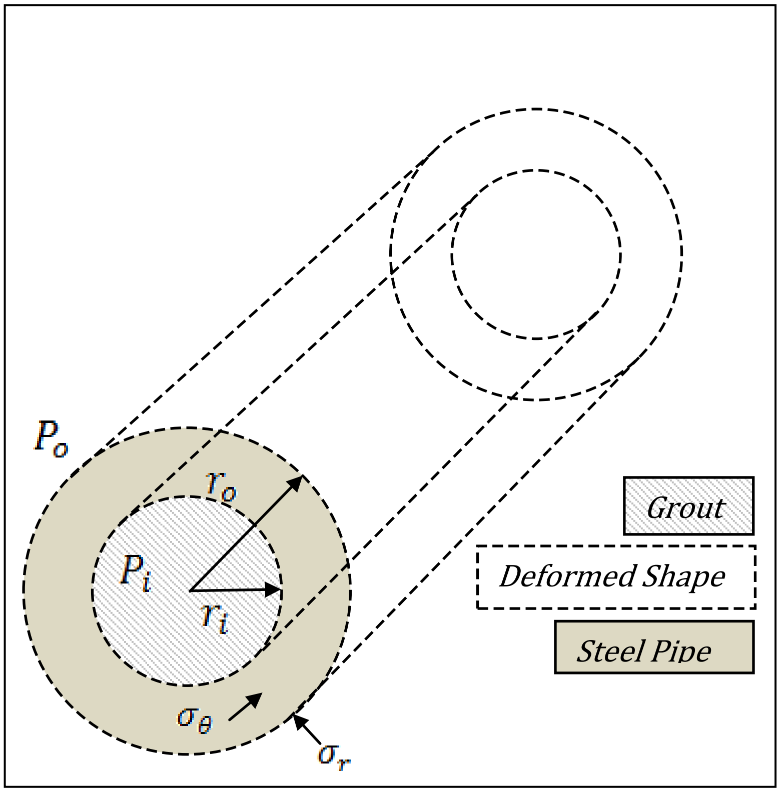

Figure 4 Cylindrical setup

For axial symmetric problems, the hoop strain $\varepsilon_\theta(r)$ is related to the radial displacement $u_r(r)$ by the following relation:

$$\varepsilon_\theta(r) = \frac{u_r(r)}{r} \tag{8}$$

Also, according to Hooke's law:

$$\varepsilon_\theta(r) = \frac{1}{E}[\sigma_\theta(r) - v\sigma_r(r) - v\sigma_z(r)] \tag{9}$$

where E and v are the steel pipe modulus and Poisson ratio respectively. It follows that the radial displacement can also be obtained from these stresses.

$$u_r(r) = \frac{r}{E}[\sigma_\theta(r) - v\sigma_r(r) - v\sigma_z(r)] \tag{10}$$

Furthermore, at the outer surface of the steel pipe, $\sigma_r(r_o) = p_o = 0;\ \ \sigma_z(r_o) = v\sigma_\theta(r_o)$ the internal pressure can be computed directly from the outer surface strain as

$$p_i = \frac{E\varepsilon_r(r_0)}{1-v^2}\frac{r_o^{\,2} - r_i^2}{2r_i^2} \tag{11}$$

Note that the internal pressure p_i is developed due to the confined expansion of the grout material within the steel pipe. In the following, we develop an explicit relation between the internal pressure, grout modulus and linear expansion coefficient. The problem can be solved using the following procedure:

1. Consider only the steel pipe under internal pressure p_i. The pipe will deform as illustrated in Fig. 5 with the interior surface displacement $u_{rs}(b)$

2. Consider only the grout material under pressure p_i, as shown in Figure 5, the grout will contract by a radial displacement of $u_{rg}(b)$

3. The gap due to displacement $u_{rs}(b)$ and $u_{rg}(b)$ will be filled by grout expansion. Explicit solution associated with this procedure is given below

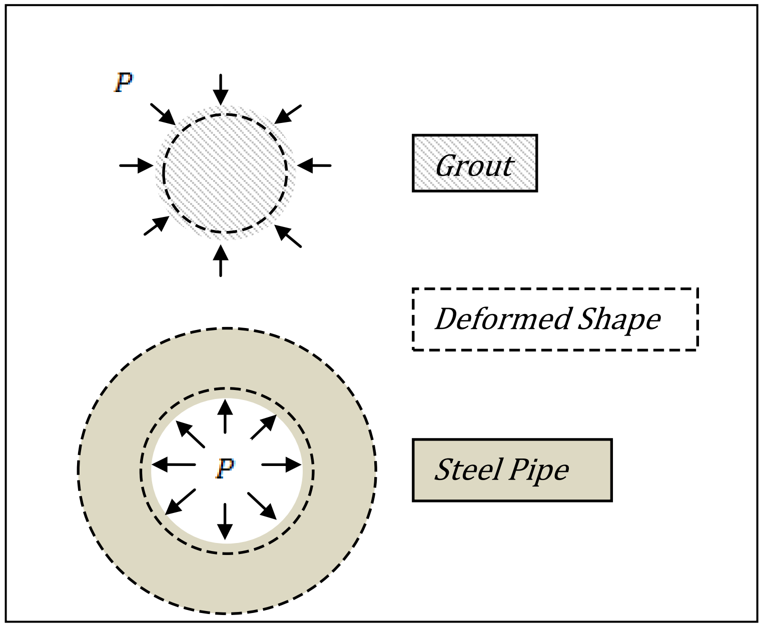

Figure 5 Deformations due to pressure

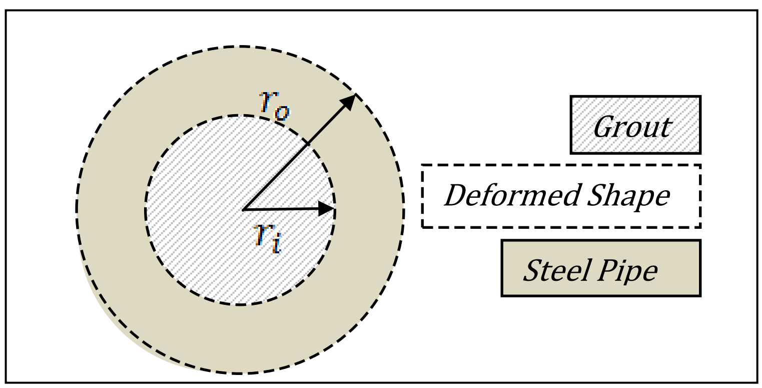

Figure 6 Radii definitions $r_i = b$ and $r_o = c$

For steel pipe

$$r_i = b \quad r_o = c$$

$$p_i = p \quad p_o = 0$$

$$\sigma_{rs}(b) = -p;\ \sigma_{\theta s}(b) = \frac{b^2 + c^2}{c^2 - b^2} p;\quad \sigma_{zs}(b) = \frac{2b^2}{c^2 - b^2} p\nu_s \tag{12}$$

here the subscript "s" is for steel. For the grout material $r_i = 0 \;\; r_o = b$ and it is under hydrostatic stress condition (plane strain).

$$\sigma_{rg}(b) = \sigma_{\theta g}(b) = -p;\quad \sigma_{zg}(b) = -2p\nu_g \tag{13}$$

Here the subscript "g" is for grout. The radial deformations in steel pipe and in the grout at $r = b$ are

$$u_{r_i s} = \frac{b}{E_s}\left(\sigma_{\theta s}(b) - \nu_s \sigma_{rs}(b) - \nu_s \sigma_{zs}(b)\right) \tag{14}$$

$$u_{r_o g} = \frac{b}{E_g}\left(\sigma_{\theta g}(b) - \nu_g \sigma_{rg}(b) - \nu_g \sigma_{zg}(b)\right) \tag{15}$$

substituting stress relations we have:

$$u_{r_i s} = \frac{pb}{E_s}\left(\frac{b^2 + c^2}{c^2 - b^2} + \nu_s - \frac{2b^2}{c^2 - b^2}\nu_s^2\right) \tag{16}$$

$$u_{r_o g} = -\frac{b}{E_g}\left(1 - \nu_g - 2\nu_g^2\right) p \tag{17}$$

The continuity equation as discussed in step 3 gives

$$\Delta u_r = u_{r_i s}(b) - u_{r_o g}(b) = b(1 + \nu_g)\alpha \tag{18}$$

the difference in radial expansions can also be expressed as:

$$\Delta u_r = \frac{pb}{E_g}\left(1-\nu_g - 2\nu_g^2\right) + \frac{pb}{E_s}\left(\frac{b^2+c^2}{c^2-b^2} + \nu_s - \frac{2b^2}{c^2-b^2}\nu_s^2\right) \tag{19}$$

Eq. (18) and Eq. (19) are set equal to solve for α, the linear expansion coefficient of the grout material. Thus a direct relation between internal pressure p and grout material properties can be obtained:

$$\alpha = \frac{p}{E_g}\frac{1-\nu_g-2\nu_g{}^2}{1+\nu_g} + \frac{p}{E_s}\frac{1}{1+\nu_g}\left(\frac{b^2+c^2}{c^2-b^2} + \nu_s - \frac{2b^2}{c^2-b^2}\nu_s{}^2\right) \tag{20}$$

Note that the internal pressure p can be obtained from Eq. (11) as

$$p = \frac{E_s \varepsilon_\theta(c)}{1-\nu_s{}^2}\frac{c^2-b^2}{2b^2} \tag{21}$$

hence

$$\alpha = \varepsilon_\theta(c)\frac{c^2-b^2}{2b^2}\left[\frac{E_s}{E_g}\frac{1-\nu_g-2\nu_g{}^2}{(1+\nu_g)(1-\nu_s{}^2)} + \frac{1}{(1+\nu_g)(1-\nu_s{}^2)}\left(\frac{b^2+c^2}{c^2-b^2}+\nu_s-\frac{2b^2}{c^2-b^2}\nu_s{}^2\right)\right] \tag{22}$$

Eq. (22) relates the measurable hoop strain $\varepsilon_\theta(c)$ at outer surface of the steel pipe with grout material properties E_g, ν_g, and α. Since the Poisson's ratio ν_g is of secondary importance in developing the grout pressure, in the following we take a typical value of $\nu_g = 0.3$. Then the remaining material constants E_g and α can be determined from two sets of different steel pipe geometries as follows.

$$\text{Pipe 1: } A_1 = \frac{c_1{}^2}{c_1{}^2-b_1{}^2};\;\; B_1 = \frac{b_1{}^2}{c_1{}^2-b_1{}^2}$$

$$\text{Pipe 2: } A_2 = \frac{c_2{}^2}{c_2{}^2-b_2{}^2};\;\; B_2 = \frac{b_2{}^2}{c_2{}^2-b_2{}^2}$$

then

$$\begin{aligned}\alpha &= \frac{\varepsilon_{\theta 1}}{2B_1}\left[\frac{E_s}{E_g}\frac{1-v_g-2v_g^{\ 2}}{(1+v_g)(1-v_s^{\ 2})}+\frac{1}{(1+v_g)(1-v_s^{\ 2})}\left((A_1+B_1+v_s-2B_1v_s^{\ 2}\right)\right]\\ &= \frac{\varepsilon_{\theta 2}}{2B_2}\left[\frac{E_s}{E_g}\frac{1-v_g-2v_g^{\ 2}}{(1+v_g)(1-v_s^{\ 2})}+\frac{1}{(1+v_g)(1-v_s^{\ 2})}\left((A_2+B_2+v_s-2B_2v_s^{\ 2}\right)\right]\end{aligned} \tag{23}$$

From Eq. (23) the grout modulus can be solved

$$\frac{E_g}{E_s}=\frac{(1-v_g-2v_g^{\ 2})(\varepsilon_{\theta 2}B_1/\varepsilon_{\theta 1}B_2-1)}{[(A_1+B_1)(1-v_s)-2B_1v_s^{\ 2}]-(\varepsilon_{\theta 2}B_1/\varepsilon_{\theta 1}B_2)[(A_2+B_2+v_s-2B_2v_s^{\ 2}]} \tag{24}$$

once E_g is known, α can be obtained from either expression in Eq. (23).

From Eq. (23) and Eq. (24) it is seen that once the outer surface hoop strains $\varepsilon_\theta(c)$ are measured from two different steel pipes, the grout modulus E_g and linear expansion coefficient α can be uniquely determined. These two equations thus form the basis for the experimental investigation in next chapter.

CHAPTER 3: EXPERIMENTAL RESULTS

3.1 Test Setup

The experimental work undertaken in this study consisted of measuring the resulting circumferential strain from two different pipe-grout systems. Steel pipes were chosen based on their composition and dimensions. The first pipe tested was a two inch schedule forty pipe, this resulted in the grout ejecting itself from the pipe after about twelve hours curing. This was later determined to be due to the low level of confinement by the steel. For successful expansion experiments the ratio of steel to grout must be higher than that of the two inch schedule forty pipe experiment. All subsequent tests used steel pipes with thicker walls and smaller diameters. All pipes were cut to a length ten times their diameter. This was to remove the possibility of any end effects on the measurements. All measurements used for calculating material properties were taken at the midpoint of all test specimens. For the preliminary tests however several strain measurements were recorded along the length of the pipe to investigate the pressure distribution.

It should be noted that for any future work it is critical that the grout be kept in an airtight dry place. Several tests were conducted that had low levels of expansion which was ultimately found to be a result of the grout being spoiled. For the application of strain gauges on the pipes, a standard procedure was undertaken:

1. Wire brush surface to remove any coating
2. Clean with a medium grit sandpaper
3. Wipe surface with acetone to remove any oil
4. Apply strain gauge conditioner, wait until dry
5. Apply strain gauge neutralizer, wait until dry
6. Use cyanoacrylate glue to adhere strain gauge to pipe

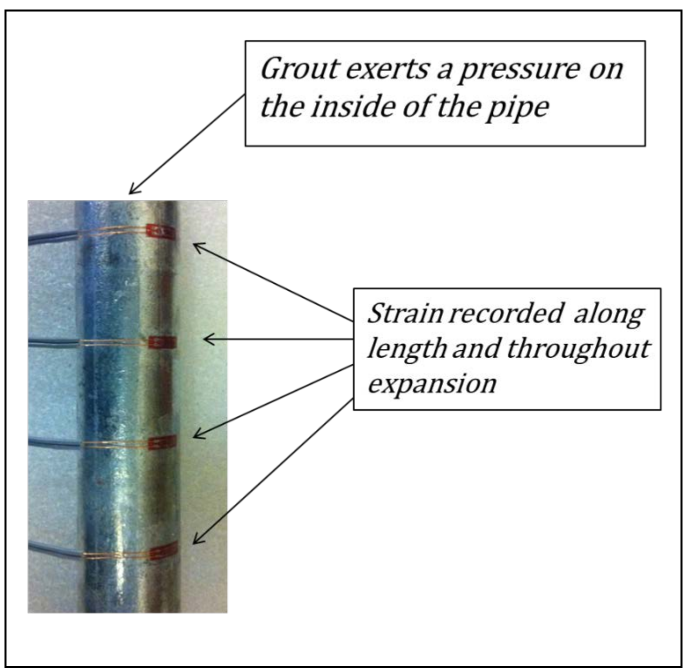

Figure 7 Strain gauge layout

Figure 8 Pipe filled with grout

Figure 7 shows an example of a preliminary test with four strain gauges distributed along the outer surface of the steel pipe. The instrumented steel pipe was then stabilized in a sand pile to avoid environmental effects.

Pipe sizes tested are given in the table below. They were selected for their availability and size. They are formed by an extrusion process, which means they are seamless and held to very tight tolerances. Pipes showing large variation in dimensions would be unsuitable for the experimentation done in this work.

Pipe Size	r_i	r_o
Small	0.250	0.500
Medium	0.375	0.625
Large	0.375	0.750

Table 1 Pipe sizes

Once the strain gauges were installed they were connected to a compact data acquisition system for calibration and data capture. For this a National Instruments ® cDAQ-9174 as shown in Figure 9 was used. This is a universal serial bus data acquisition system that logs data to a computer through a USB cable. The acquisition software used was LabVIEW®. This required building a custom virtual instrument. An important feature of this customized virtual instrument was its ability to sample data at a rate much lower than the system default. The sampling rate was 0.083 Hertz and the data was written to a text file for analysis.

Figure 9 NI cDAQ-9174

3.2 Experimental Results

For each expansive grout filled steel pipe, data was collected over the course of several days. The majority of the pipes were recorded for six and a half days. This length of time was determined from preliminary tests that determined the curing time at which the expansion level would taper off. Interestingly, in literature pertaining to expanding grout based grips it is only recommend to allow the expansive grout to cure for three days. The results were smoothed using a MATLAB ® “smooth” function, this was very effective in removing noise from the recorded signal.

Figure 10 gives the measured outer surface hoop strains for two steel pipes graphed versus time. For each pipe, strains at four locations were measured simultaneously and recorded to 6.5 days. The hoop strain at the uncapped end is distinctive smaller than all other locations because the grout material is relatively free to expand (overflowing into a pulverized heap). About 2 diameters distance away from the free end, the plane strain condition has been fully established. This can be seen from the fact that the measured strains there is almost identical to those measured at midsection and capped end of the pipe. We note that the gradual application up of pressure from the uncapped end is an effective way of eliminating unwanted stress concentration at the free end, which will be beneficial to large composite specimen testing as discussed in Chapter 2.

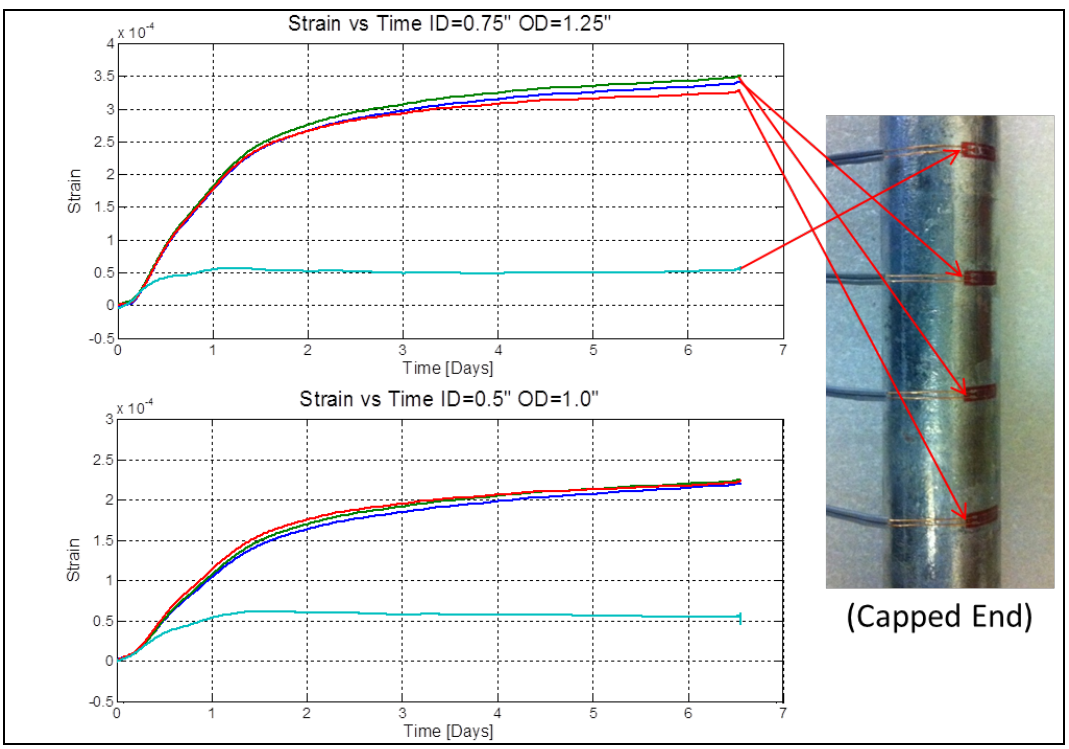

Figure 10 Data strain versus time

Through the strain measurements it was also seen that the grout material away from the free (uncapped) end, continued to expand even after 6 days, although after the first three days (72 hours) the strain buildup slows down significantly. In contrast, the strain reading near the free end appears to relax after two days. It is unclear what caused the strain drop at the free end. It is suspected that the ambient moisture incursion might be responsible for it. If this is true, extra precautions must be observed when applying such expansive grout materials for permanent structural supporting purposes. To gather further data pertaining to this phenomenon the strain is being recorded past the 6.5 day mark, but data analysis on this long duration experiments will not be included in this study.

The recorded strains are fairly consistent with different tests. Table 2 and Table 3 list the averaged hoops strains as function of time for two different pipe systems.

Days	Large [με]	Medium [με]
1	140	223
2	167	273
3	187	303
4	196	315
5	207	328
6	214	335
6.5	217	340

Table 2 Strain for the Large-Medium system

Days	Medium [με]	Small [με]
1	209	125
2	280	173
3	310	193
4	328	206
5	338	215
6	344	220
6.5	352	225

Table 3 Strain for Medium-Small system

The relative strain levels followed what is expected, the maximum pressure developed at the grout-steel interface was around ten thousand pounds per square inch (psi). This agrees well with the maximum pressure as advertised by the manufacturer of the expansive grout. With these strain values entered into Eq. (23) and Eq. (24) the expansion coefficient and grout modulus can be calculated for both systems of pipes. For the Small-Medium Pipe system, the medium pipe developed a pressure of ~11000 psi, the small pipe developed a pressure of ~10000 psi. Solving the small-medium system using Eq. (23) and Eq. (24) gives (after 6.5 days):

$$\alpha \cong 0.1502\ \% \qquad and \qquad E_g \cong 4.45 \cdot 10^6\ psi$$

For the Large-Medium Pipe system, the large pipe developed a pressure of ~10700 psi and the medium pipe developed a pressure of ~11000 psi. Solving the medium-large system gives (after 6.5 days):

$$\alpha \cong 0.1653\ \% \qquad and \qquad E_g \cong 4.59 \cdot 10^6\ psi$$

Furthermore, using Eq. (23) and Eq. (24) the properties can be solved as a function of time to investigate behavior the properties as the curing process takes place. The results are summarized in Figure 11 where E_g and α are plotted as functions of time.

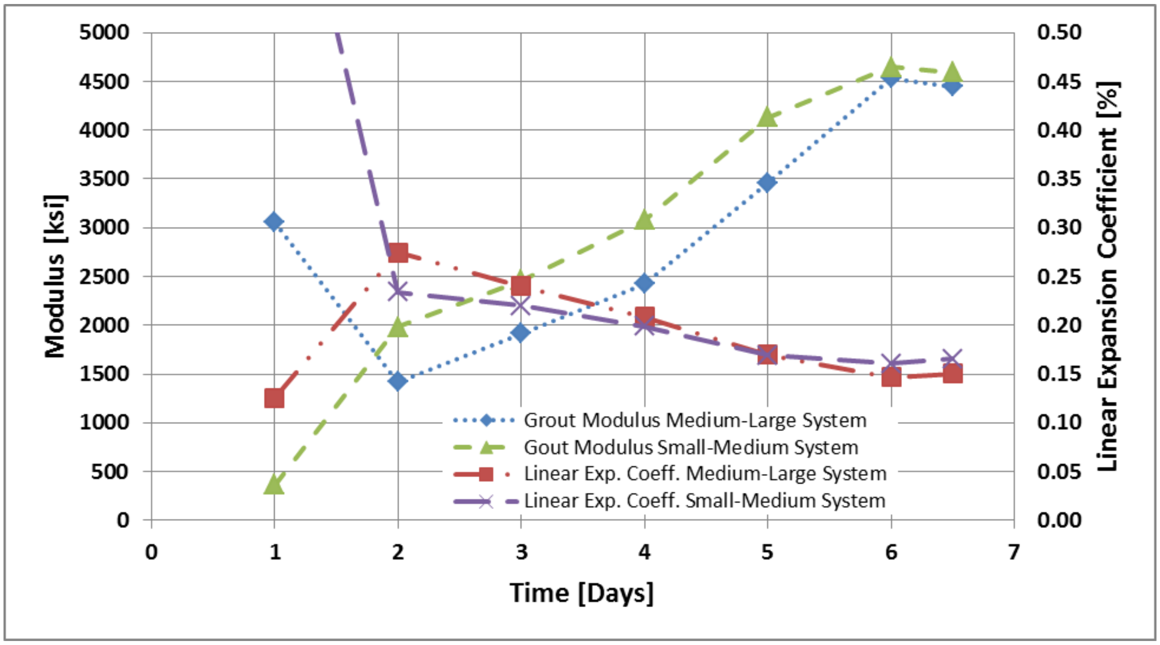

Figure 11 Properties versus Time

This graph shows that during the earlier curing stage, the material properties were not well established and exhibit large differences. However, after about 5 days, both the E_g curves and the α curves converge to stabilized values. These results suggest that the ASTM recommended three day (72 hours) may not be enough for the grout material to be fully cured. Five days (120 hours) is more reasonable in order to achieve higher gripping pressures and consistent results.

CHAPTER 4: APPLICATION TO SPECIMEN DESIGN

4.1 Analytical groundwork

In this chapter the experimentally determined properties are used to design more effective expansive grout based grips. The grip is a series of thick walled cylindrical shells. With this the fundamental equations (Eq. 4-10) can be used to work out the stresses in any expansive grout based grip system. In the figure below p_{sg} is the pressure between the steel pipe and expansive grout, and p_{gc} is the pressure between the expansive grout and composite specimen, i.e. gripping pressure.

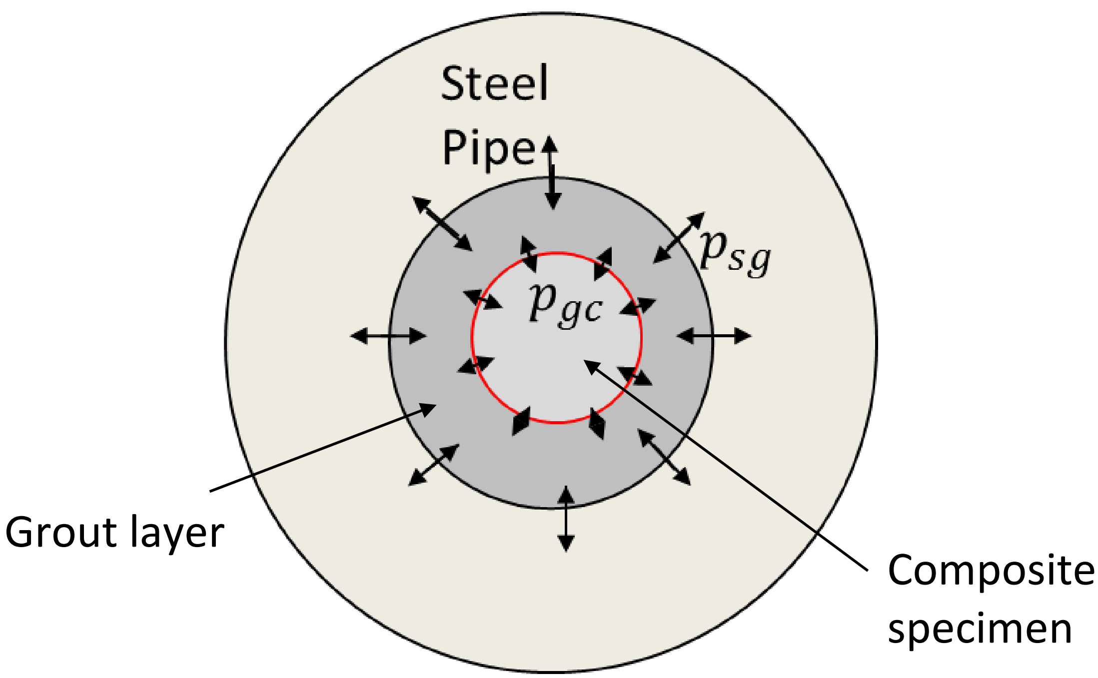

Figure 11 Cross Section with composite specimen

The approach is similar to the procedure in the previous chapter. The unknowns in this case are the two pressures and we can generate two equations based on displacement compatibility at the two interfaces and solve for the pressures at the interfaces.

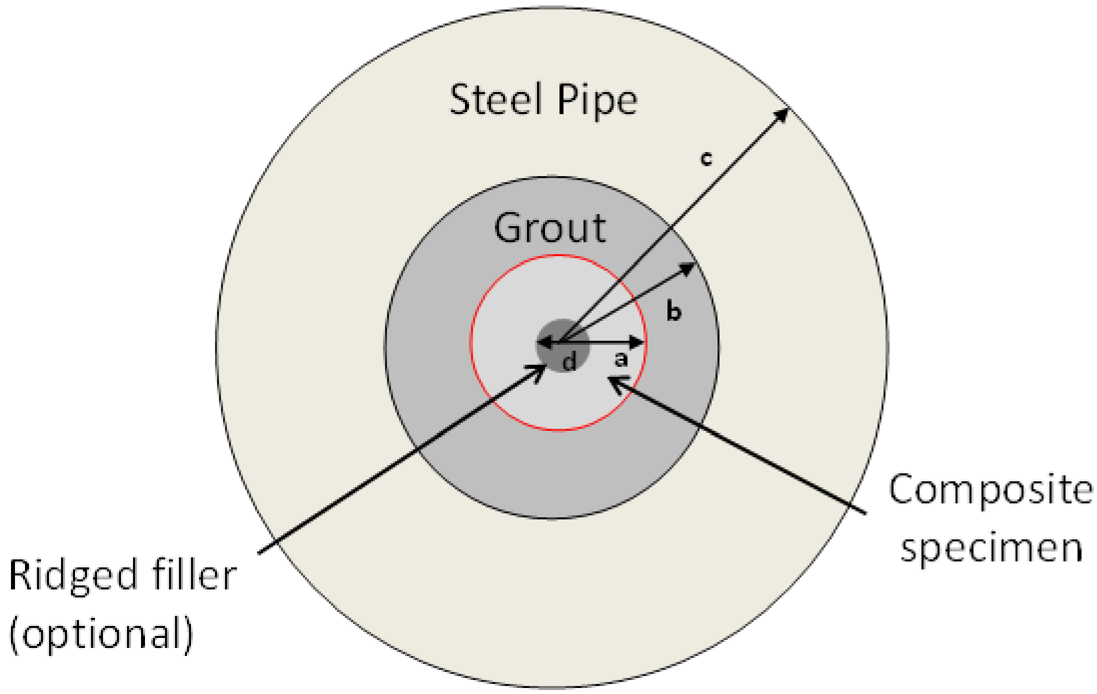

Figure 12 New radii definitions

Based on the thick walled cylinder equations we can express the displacements as functions of the pressure. For the general equation we have:

$$\sigma_r(r) = \frac{P_i r_i^2 - P_o r_o^2 + \left(\frac{r_i r_o}{r}\right)^2 (P_o - P_i)}{r_o^2 - r_i^2} \tag{25}$$

$$\sigma_\theta(r) = \frac{P_i r_i^2 - P_o r_o^2 - \left(\frac{r_i r_o}{r}\right)^2 (P_o - P_i)}{r_o^2 - r_i^2} \tag{26}$$

Plane-strain condition introduces

$$\sigma_z = -2\nu \frac{P_i r_i^2 - P_o r_o^2}{r_i^2 - r_o^2} \tag{27}$$

The stress-displacement relation is

$$u_r(r) = \frac{r}{E}\left(\sigma_\theta - \nu\sigma_r - \nu\sigma_z\right) \tag{28}$$

The geometric relation from axial symmetry

$$\varepsilon_\theta = \frac{u_r}{r} \tag{29}$$

Thus the stresses and radial displacement at steel-grout interface are

$$r_i = b \quad r_o = c$$

$$P_o = 0 \quad P_i = p_{sg}$$

$$\sigma_{\theta s}(b) = p_{sg}\left(\frac{b^2 + c^2}{c^2 - b^2}\right) \tag{30}$$

$$\sigma_{rs}(b) = -p_{sg} \tag{31}$$

$$\sigma_{zs} = \frac{2b^2}{c^2 - b^2} p_{sg}\nu_s \tag{32}$$

$$u_{rs}(b) = \frac{b \cdot p_{sg}}{E_s}\left(\frac{b^2 + c^2}{c^2 - b^2} + \nu_s - \frac{2b^2}{c^2 - b^2}\nu_s^2\right) \tag{33}$$

Plugging in $C_{cb} = \dfrac{c^2}{c^2 - b^2}$ $B_{cb} = \dfrac{b^2}{c^2 - b^2}$ and simplifying yields

$$u_{rs}(b) = b\left(1 + \nu_s\right)\frac{p_{sg}}{E_s}\left(C_{cb} + B_{cb}(1 - 2\nu_s)\right) \tag{34}$$

If the composite specimen is hollow and filled with a rigid filler such as a steel rod, the composite modulus can be set artificially high to take into account the increased stiffness that the rigid filler would add. The displacement at the composite-grout interface can be derived as follows:

$$r_i = d \quad r_o = a$$

$$P_o = p_{gc} \quad P_i = 0$$

$$\sigma_{rc}(a) = -p_{gc}$$

$$\sigma_{\theta c}(a) = -p_{gc}\left(\frac{a^2+d^2}{a^2-d^2}\right) \tag{35}$$

$$\sigma_{zc} = -p_{gc}\frac{2a^2}{a^2-d^2}\nu_c \tag{36}$$

Plugging into stress-displacement relation and substituting

$$A_{ad} = \frac{a^2}{a^2-d^2} \quad D_{ad} = \frac{d^2}{a^2-d^2}$$

displacement expression for the composite at grout interface becomes

$$u_{rc}(a) = -a(1+\nu_c)\frac{p_{gc}}{E_c}(D_{ad} + A_{ad}(1-2\nu_c)) \tag{37}$$

with these two equations (Eq. 34 and Eq. 37) for the displacements at the steel grout interface and the grout composite interface as functions of pressure, we consider the displacements as functions of the linear expansion of the grout. This is accomplished by adding an expansion term to the strain and expressing this as a displacement from our axial symmetric assumption. Setting these displacements equal to the displacements from Eq. (34) and Eq. (37) the pressures can be solved for, the strain based displacement equations are now derived.

For the grout layer

$$r_i = a \;\; r_o = b$$

$$P_o = p_{sg} \quad P_i = p_{gc}$$

$$\sigma_{rg}\left(r\right) = \frac{p_{gc}a^2 - p_{sg}b^2 + \left(\frac{ab}{r}\right)^2 \left(p_{sg} - p_{gc}\right)}{a^2 - b^2} \tag{38}$$

$$\sigma_{\theta g}\left(r\right) = \frac{p_{gc}a^2 - p_{sg}b^2 - \left(\frac{ab}{r}\right)^2 \left(p_{sg} - p_{gc}\right)}{a^2 - b^2} \tag{39}$$

$$\sigma_{zg}\left(r\right) = -2\nu_g \frac{p_{gc}a^2 - p_{sg}b^2}{a^2 - b^2} \tag{40}$$

plugging into Hooke's Law

$$u_{rg}\left(r\right) = \frac{r}{E_g}\left(\sigma_\theta^g(r) - \nu\sigma_r^g(r) - \nu\sigma_z^g(r)\right) \tag{41}$$

then expressing as circumferential strain and adding the linear expansion term

$$\varepsilon_{\theta g}\left(r\right) = \frac{u_{rg}\left(r\right)}{r} + \left(1 + \nu_g\right)\alpha \tag{42}$$

then the new displacement becomes:

$$u_{rg}\left(r\right)^* = r\left(\frac{u_{rg}\left(r\right)}{r} + \left(1 + \nu_g\right)\alpha\right) \tag{43}$$

Here we introduce $B_{ba} = \frac{b^2}{b^2 - a^2}$ $A_{ba} = \frac{a^2}{b^2 - a^2}$ and simplify $u_{rg}\left(r\right)^*$ at a and b

$$u_{rg}\left(a\right)^* = a\left(\left(1 + \nu_g\right)\left(B_{ba} + A_{ba}\left(1 - 2\nu_g\right)\right)\frac{p_{gc}}{E_g} - 2\left(1 + \nu_g\right)\left(1 - \nu_g\right)B_{ba}\frac{p_{sg}}{E_g} + \alpha\left(1 + \nu_g\right)\right) \tag{44}$$

$$u_{rg}\left(b\right)^{*}=b\left(2\left(1+\nu_{g}\right)\left(1-\nu_{g}\right)A_{ba}\frac{p_{gc}}{E_{g}}-\left(1+\nu_{g}\right)\left(A_{ba}+B_{ba}\left(1-2\nu_{g}\right)\right)\frac{p_{sg}}{E_{g}}+\alpha\left(1+\nu_{g}\right)\right) \quad (45)$$

now we set $u_{rg}\left(a\right)^{*}=u_{rc}\left(a\right)$ and $u_{rg}\left(b\right)^{*}=u_{rs}(b)$ we can now solve for p_{gc} by eliminating p_{sg}

$$p_{gc}=\frac{E_{g}\alpha\left(1+\nu_{g}\right)\left(E_{s}\left(A_{ab}-B_{ba}\right)\left(1+\nu_{g}\right)+E_{g}\left(B_{cb}+C_{cb}-B_{cb}\nu_{s}+C_{cb}\nu_{s}-2B_{cb}\nu_{s}^{2}\right)\right)}{E_{s}(4A_{ba}B_{ba}\left(\nu_{g}^{2}-1\right)^{2}+\left(\left(1+\nu_{g}\right)\left(A_{ba}+B_{ba}-2A_{ba}\nu_{g}\right)+\frac{E_{g}\left(D_{ad}+A_{ad}-2A_{ad}\nu_{c}\right)\left(1+\nu_{s}\right)}{E_{c}}\right)\left(-\left(1+\nu_{g}\right)\left(A_{ba}+B_{ba}-2B_{ba}\nu_{g}\right)-\frac{E_{g}\left(B_{cb}+C_{cb}-2D_{ad}\nu_{c}\right)\left(1+\nu_{s}\right)}{E_{s}}\right)} \quad (46)$$

4.2 Real Applications

Now the system is fully solved and all stresses and displacements can be calculated for any point within the system. This will allow for intelligent design of future grip systems. In this section we will examine a past design that was found through trial and error, which was very time consuming and expensive. This testing has been successfully completed at the Structural Laboratory at the Civil, Architectural, and Environmental Engineering Department of the University of Miami, Coral Gables, FL. The tensile tests were performed using a 200 kip Baldwin universal testing frame. The bottom expansive grout based grip was wedge-gripped to the machine base and the top of the specimen was anchored to the machine head both shown in Figure 14. The specimens had an outside diameter of 0.8 inch, the pipe that was found to provide adequate gripping was a one and one half inch schedule forty pipe, cut to a length of fifteen inches. These dimensions and the failure loads can give us an effective friction coefficient that can be used as a lower bound for future designs. This will be relatively conservative, because with different surface treatments on the composite rod these values could show a great deal of variation.

Specimen	Length of grip [in]	Failure load [lbf]	F_τ [psi]	p_{gc} [psi]	μ_s
Green Bar #1	15	34,331	728.55	1,020	0.7143
Green Bar #2	15	29,226	620.21	1,020	0.6081
Basalt Bar #1	15	34,371	729.40	1,020	0.7151
Basalt Bar #2	15	38,310	812.99	1,020	0.7970
Glass Bar #1	15	35,835	760.46	1,020	0.7456
Glass Bar #2	15	38,041	807.28	1,020	0.7914
Average		35,019	743.15		0.7286
Standard Deviation		3319.1	64.298		0.0630
Coeff. Of variation [%]		9.4779	8.6521		8.6521

Table 4 Effective friction coefficients

Figure 13 Test setup

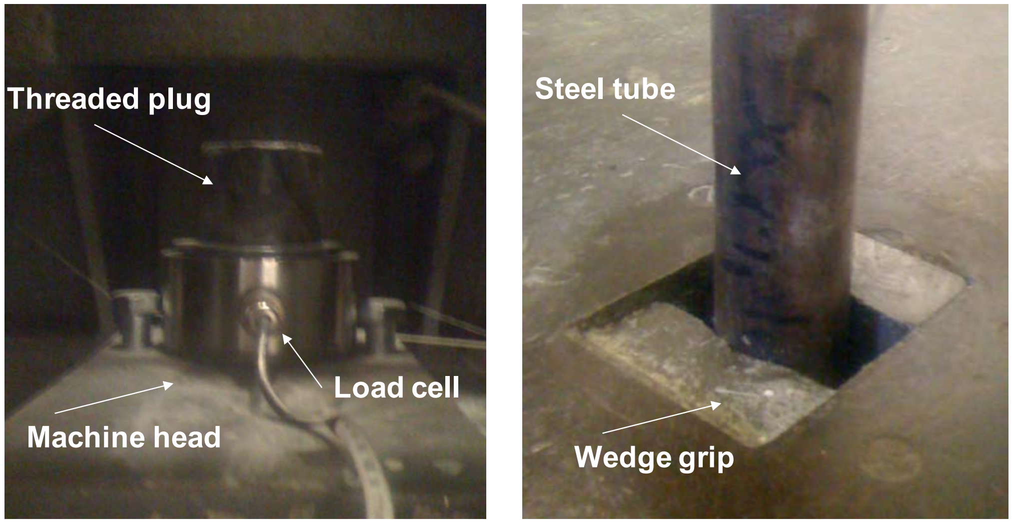

Figure 14 Anchorage to test machine

With the equation for the grout-composite pressure, pipes can be chosen for arbitrary composite specimens such that the pressure developed by the expansive grout is maximized. In Figure 15 the pressure is plotted versus grout shell thickness, while steel wall thickness and composite diameter are fixed.

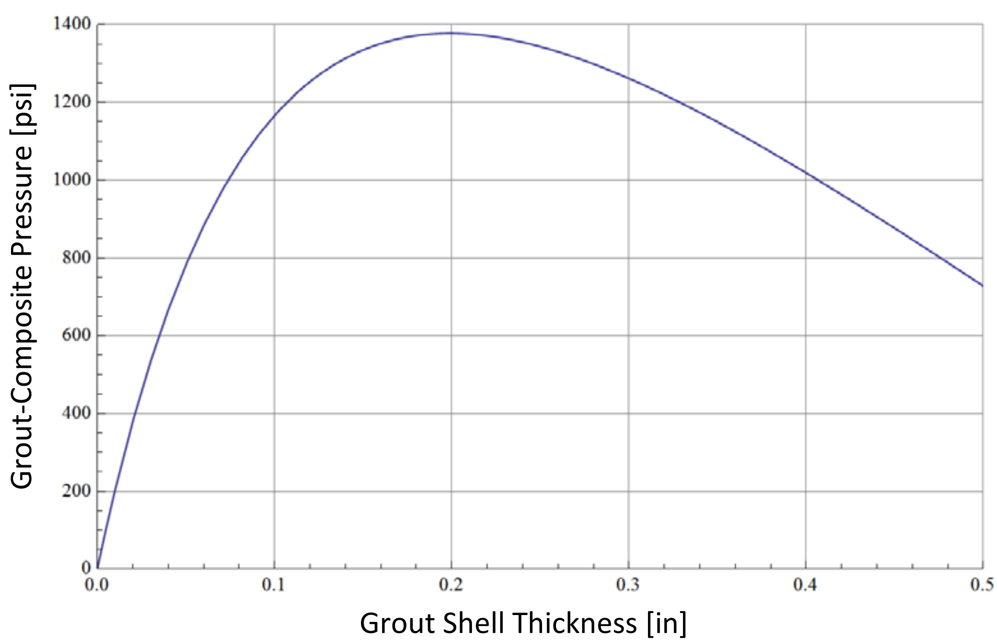

Figure 15 Optimal grout shell thickness

From this graph it can be seen that the optimal grout shell thickness is 0.19” with a pressure of 1380 psi. In the grip design that was used the grout shell thickness was 0.41” more than twice the optimal, as a result the pressure developed was only 1020 psi. To reduce the grout shell thickness, one size smaller pipe (1-1/4” SCH 40) could be used and would increase the pressure to 1250 psi as well as reduce the volume of steel by sixteen percent. With this new higher pressure, the grip length could have been reduced by eighteen percent. With these two design changes the steel could be reduced in each grip by thirty two percent and the amount of grout reduced by thirty five percent. This would lead to significant savings and still represents a conservative design because the friction coefficients in actuality are higher. This upper bound was not established because the grout composite interface never reached a critical level.

CHAPTER 5: CONCLUSIONS AND RECOMMENDATIONS

5.1 Design Guidelines

The main contribution of this work is the development of a design guideline to assist in the future fabrication of expansive grout based grips for large scale composites testing. In the design of a future grip system there are a number of factors to take into account.

1. The pressure developed on the composite should be maximized
2. An estimated effective friction coefficient is needed
3. Must know pipe size availability
4. Estimated failure load

For a designer the first consideration is what pipe to select, from the grout shell thickness graph it is clear that as the grout shell thickness increases the pressure transferred to the composite specimen decreases significantly. In the graph presented below Figure 16, maximum pressures can be read for various pipes as functions of composite specimen radii.

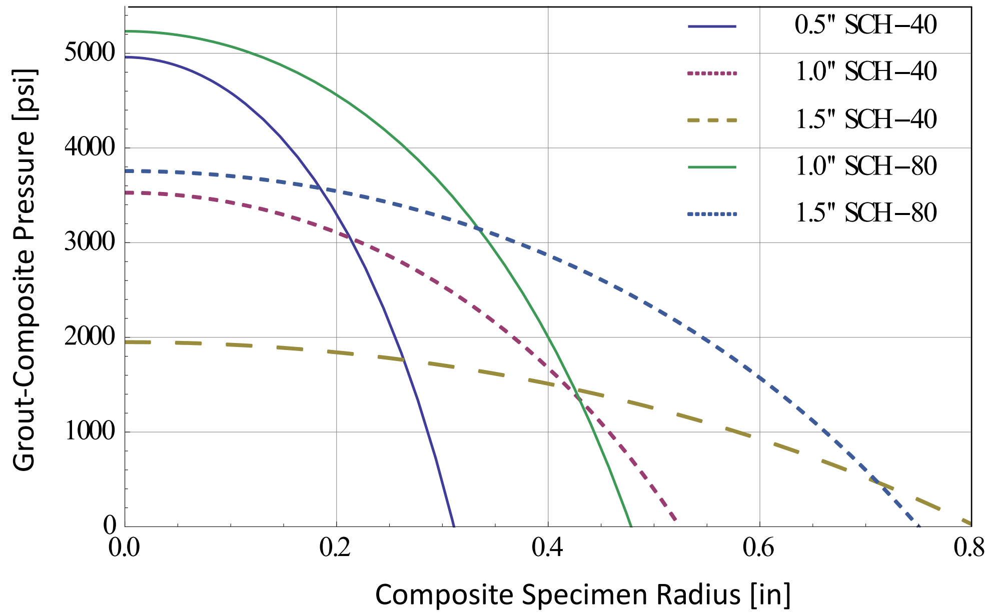

Figure 16 Grout-Composite Pressure vs. Composite Radii

In order to maximize the grout composite pressure for a given specimen the pipe corresponding to the highest pressure should be chosen. The next and equally critical parameter is the length of pipe to be used. A very high pressure would do little good if it were only applied over a short length. Ultimately our goal remains to develop enough traction or gripping force to reach the ultimate stress level in the gage section. An optimal grip will develop a high gripping pressure so that the grip length is not excessive. As stated before the effective friction coefficient is bar specific, meaning that friction values calculated in this work may not be valid for another bar, but if a grip-specimen configuration were to slip the next iteration could insure this level of interfacial stress does not reach a critical level. For the next graph the estimated friction coefficients are used from the testing we have completed in the past. The lengths are determined by manipulation of the simple equation:

$$F_u = p_{gc} \cdot A \cdot \mu_s \tag{47}$$

Where F_u is the ultimate tensile force, A is the area of the grout-composite interface, and μ_s is the estimated friction coefficient, and a is the composite radius, rearranging

$$A = 2a\pi L \tag{48}$$

$$p_{gc} = \frac{F_u}{2a\pi\mu_s}\frac{1}{L} \tag{49}$$

we define $C_f = \dfrac{F_u}{2a\pi\mu_s}$ and plot p_{gc} *vs.* L for various C_f values

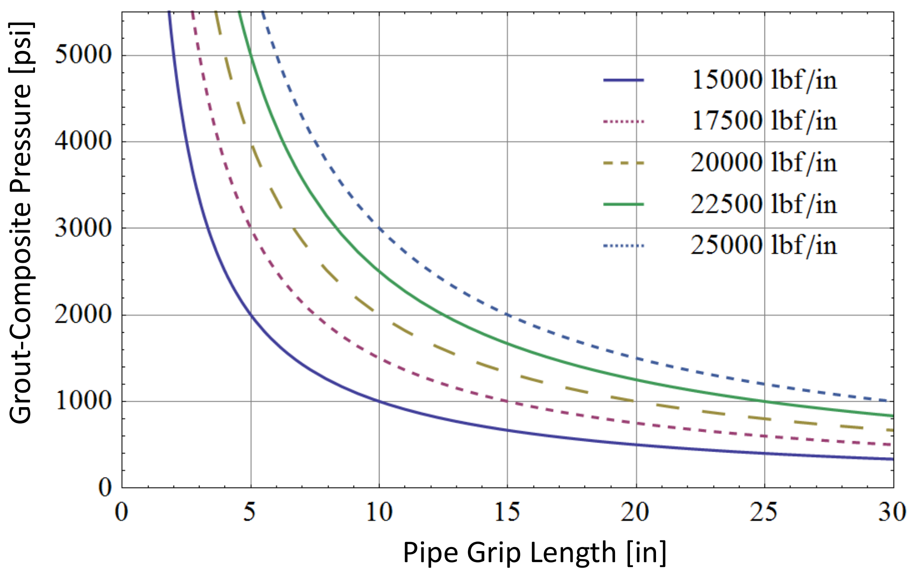

Figure 17 Pipe length chart

Combining these two graphs into a readable design guide, the pipe length chart is reflected about the y-axis and combined with the p_{gc} *vs.* a chart.

This combined chart can be used with an assumed effective friction coefficient and estimated failure load to select a pipe and corresponding pipe length.

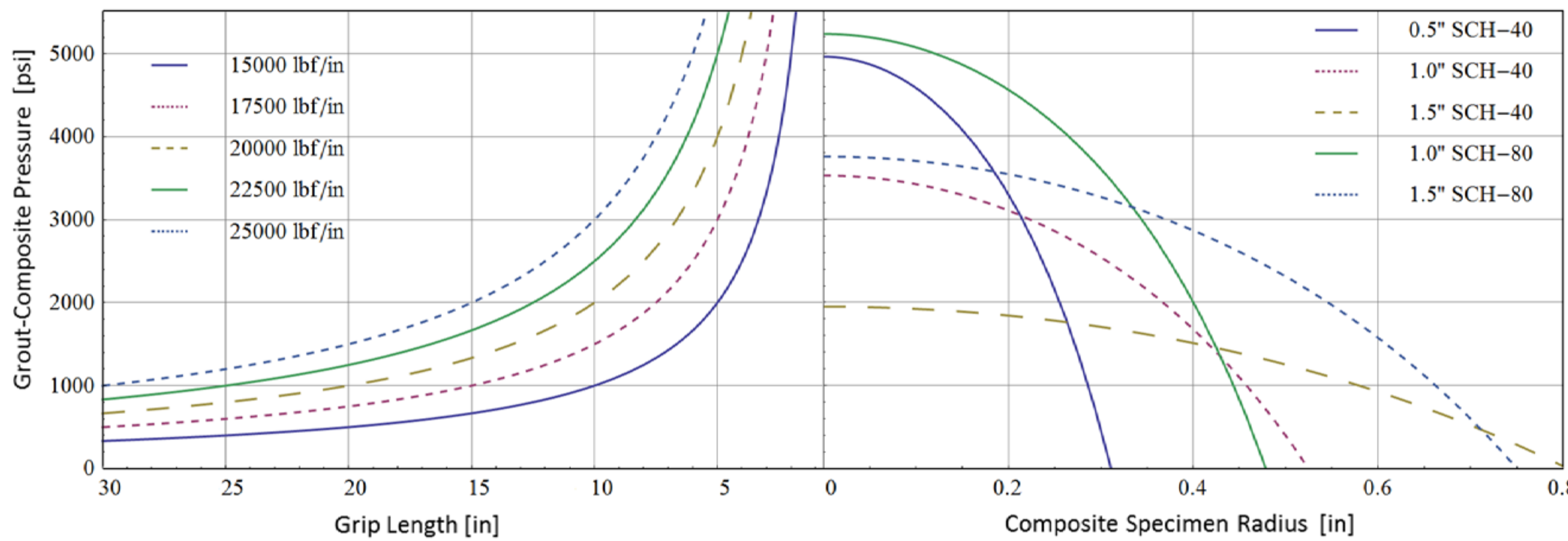

6.2 Design Guideline Example

To illustrate how this chart can be used, we will do a hypothetical design using what information we have gathered so far. Assume we have a specimen to be tested that has a radius of $0.65\ in$ and $F_u \approx 100{,}000\,lbf$.

$$Select\,line\,for\,left\,hand\,graph = \frac{F_u}{2\pi\mu_s a} = \frac{100{,}000}{2\pi \cdot 0.92 \cdot 0.65} = 26{,}614\left[\frac{lbf}{in}\right]$$

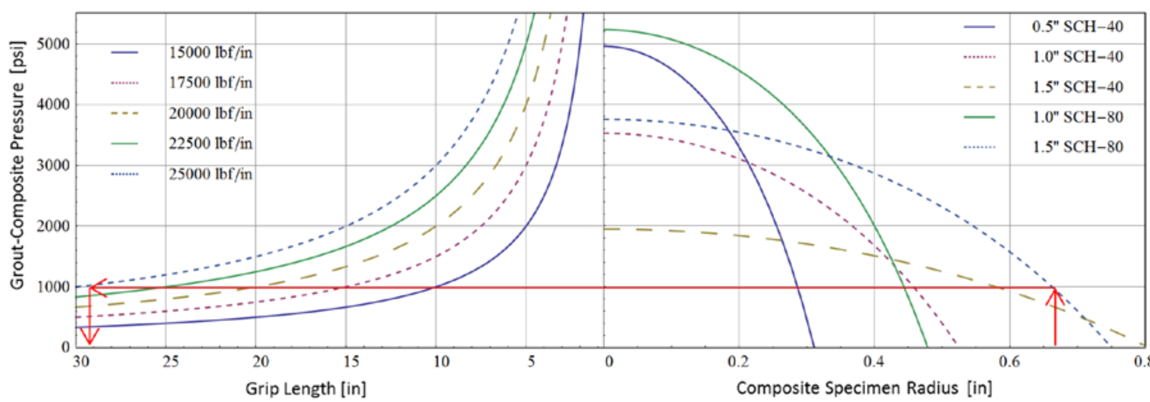

Figure 18 Example pipe design

$$Recommended\,Grip\,Length \rightarrow 29\,in$$

If this chart had been available to design the grips in a recent large scale composites characterization test, several months could have been saved as well as thousands of dollars in both time and materials. The initial length of these new grips was only twenty inches. Through a similar procedure as outlined above the grips are recommended to be at least thirty inches. The twenty inch grip suffered a slippage failure, which gave a critical interface friction coefficient of about 0.96 ; with this information the next grip can be designed so that this critical level is not reached and lead to a successful test.

6.3 Design Conclusions

With the testing and analysis completed in this work the original objectives have been completed. The design guideline provides a systematic methodology for designing expansive grout based grips and the calculated properties of the grout enable further development of this methodology. It was also found that the expanding grout should be allowed to cure for at least six days in standard laboratory conditions to allow the grout to fully expand. Future work to be considered includes finite element modeling and a study of the complex stress state within the composite specimen at and near the grip. A long term study is also suggested to investigate possible creep behavior in the expanding grout material.

BIBLIOGRAPHY

A. Al-Mayah, K. Soudki, A. Plumtree. "Novel Anchor System for CFRP Rod: Finite-Element and Mathematical Models." *Journal of Composites for Construction*, 2007: 469-476.

Budyas, Richard G. *Advanced Strength and Applied Stress Analysis.* Thomas Casson, 1999.

Daniel, Isaac M. *Engineering Mechanics of Composite Materials.* New York: Oxford University Press, 2006.

G. Portnov, C.E. Bakis. "Analysis of Stress Concentration During Tension of Round Pultruded Composite Rods." *Composite Structures 83* (Elsevier Ltd.), 2008: 100-109.

Gilstrap, J. M., Dolan, C. W., and Hamilton, H. R., III. *Characterization of Fiber Reinforced Polymer Prestressing Tendons.* Federal Highway Administration, 2001.

Jones, Robert M. *Mechanics of Composite Materials.* New York: Taylor & Francis Group, 1999.

Meier, U. "Extending the Life of Cables by the use of Carbon Fibers." *Proc., International Association for Bridge and Structural Engineering Symp.* 1995. 1235–1240.

Micelli F, Nanni A. " Mechanical Properties and Durability of FRP Rods." *Construction and Building Materials*, 2004.

Rostàsy, F. S. "FRP Tensile Elements for Prestressed Concrete: State of the Art, Potentials and Limits." *ACI Special Publication - 138*, 1993: 347–365.

S. Kocaoz, V.A. Samarnayake, A. Nanni. "Tensile Characterization of Glass FRP Bars." *Composites Part B*, 2005: 127-134.

Sadd, Martin H. *Elasticity.* Burlington: Academic Press, 2009.

Tibbets, Andrew J. "Durable Fiber Reinforced Polymer Connections for Precast Cconcrete Structures." *Master of Science Thesis*, 2008.

Valter Carvelli, Giulia Fava, Marco A. Pisani. "Anchor System for Tension Testing of Large Diameter GFRP Bars." *Journal of Composites For Construction*, 2009.